



Nanomole Silver Detection in Chloride-Free Phosphate Buffer Using Platinum and Gold Micro- and Nanoelectrodes

Prabhakar Sidamaram^{1,*} and John Colleran^{1,2,z}

¹Applied Electrochemistry Group, FOCAS Research Institute, Technological University Dublin, Dublin 8, Ireland

²School of Chemical and Pharmaceutical Sciences, Technological University Dublin, Dublin 8, Ireland

The electrochemical determination of ultra-low concentrations of silver requires reliable, reproducible measurements using sensitive analytical techniques. To date, the electrochemical determination of silver in biological buffers and pH neutral media has not been successful in terms of reproducibility. In this work, we report on the determination of ultra-low concentrations of silver in chloride-free phosphate buffer solution (PB, pH 7.4). Detection was conducted at gold and platinum micro and nanoelectrodes using anodic stripping voltammetry (ASV). The micro and nanoelectrodes were fabricated using a Sutter P-2000 laser puller, with physical and electrochemical characterization revealing flat disk-shaped working surfaces of 10–15 μm (microelectrode) and 10–100 nm (nanoelectrodes) in radius. These dimensions were calculated from steady-state limiting currents and confirmed using FE-SEM. The laser pulled electrodes exhibit excellent electrochemical activity when characterized using ferrocene, without the addition of supporting electrolyte, and reproducible stripping voltammetric profiles for the determination of silver, with a LoD of 1.3 pM (1.8%) were obtained in 0.1 M chloride-free phosphate at platinum nanoelectrode. Determination of ultra-low concentrations of silver in chloride-free PB provides the scope to explore the mechanism of action of bioinorganic silver-based anti-bacterial, anti-fungal and anti-cancer drugs in cell media for in vitro and, potentially, in vivo analysis.

© 2019 The Electrochemical Society. [DOI: 10.1149/2.1371906jes]

Manuscript submitted January 11, 2019; revised manuscript received April 4, 2019. Published April 17, 2019.

Throughout history, the use of metal-based compounds for medicinal therapeutic purposes has been practiced. The discovery of the bioinorganic platinum-based drug, cisplatin, in the 1960's, shifted scientific interest toward metal-based compounds for medicinal applications, particularly in cancer treatment.¹ A recent significant review, highlighting the challenges associated with current platinum-based drugs, explores the potential of some transition metal-based drugs and, thus, provides an insight into the future of drug development.² There is a considerable range of bioinorganic compounds reported based on different chelating metals (Pt, Ru, Cu, Ir, Rh, Sn, and Ag) and ligands.^{3,4} Metallic silver has been widely used in many medicinal applications, namely, as antiseptics, anti-microbial, and anti-inflammatory drugs.⁵ Bioinorganic silver compounds have also risen to prominence in recent years, due to their potential in cancer therapy.^{6,7} Some bioinorganic compounds are known to generate free radicals and can directly bind to DNA, inhibiting cell replication and cell division, and can actively induce apoptosis.^{8,9} The release and dissolution of complexed silver (I) ions also plays a vital role in the anti-microbial and anti-cancer properties of silver.¹⁰ Free silver (I) ions can bind to the surface of a cell membrane and can inhibit cellular respiration or disorient the metabolic activities of the cell. Silver (I) ions are reported to have enhanced bioactivity when complexed with suitable ligands but, to date, the mechanism of action of silver complex drugs is not clearly understood.⁶ Understanding the mode of action of bioinorganic drugs can be achieved using electrochemistry. If dissociation of the bioinorganic complexes occurs in cellular media, free metal ions and organic ligands can be detected. If complexes remain intact, then the characteristic electrochemical redox behavior of the bioinorganic complex will be observed. Performing this type of electrochemical analysis, at the cellular in vitro and potentially in vivo level, should help pave the way in creating highly efficient, application-specific, silver-based bioinorganic drugs.

The detection and determination of silver has been studied extensively over the past few decades, employing several different analytical methods and materials. Among these methods, electrochemical detection of silver has several advantages, such as, low cost, experimental simplicity, equipment portability, small sample volume, and high sensitivity over other techniques.^{11–18} Electrochemistry facilitates the analysis, detection, and determination of trace metals by various techniques such as anodic stripping voltammetry (ASV), differential pulse voltammetry (DPV) and square wave anodic stripping

voltammetry (SWASV). Anodic stripping voltammetry, with background subtraction (subtractive stripping), is a very effective analytical tool that involves the pre-concentration, and deposition of the metal on the electrode surface, followed by selective oxidation of the deposited metal species during an anodic potential sweep. ASV is a very sensitive and reproducible method for the detection of trace metals at low concentrations.¹⁹ To date, the electrochemical detection and determination of ultra-low concentrations of silver in biological buffers has not been very successful.^{14,15,20} To this end, some key issues have to be addressed; the electrolyte composition, pH, and detection technique all play important roles,²¹ and the presence of chloride ions in the electrolyte system greatly influences experimental reproducibility.^{15,22,23}

Optimizing the electrochemical parameters can increase the sensitivity and selectivity of the chosen method toward the detection of ultra-low concentrations of silver in chloride-free biological buffer (PB, pH 7.4). Further enhancement arises from the performance of the electrode when scaled down to micro and nano dimensions. Nanoelectrodes have advantageous properties, such as, higher mass transfer efficiency, smaller RC cell time constants, a lower iR drop, higher signal-noise ratios, and higher current densities, when compared to conventional electrodes.²⁴ As the dimension of electrodes approaches the nanoscale, properties deviate from classical electrode chemistry. Nanoelectrodes have very high mass transfer efficiency when the diffusion layer thickness approaches the Debye length. The diffusion layer thickness varies and acts as a spherical electrode at the edge of the diffusion layer, depending on the experimental timescale.^{25,26} Micro and nanoelectrodes can be fabricated by various techniques such as electrochemical/chemical etching of fabricated electrodes followed by electrodeposition of the desired metal,²⁷ Taylor's method,²⁸ lithography for micro and nanoelectrode single/arrays,²⁹ and by the laser pulling method. The reported use of laser pulling to fabricate single micro and nanoelectrodes is summarized in Table I. In cellular conditions, concentrations of the species of interest will be low and, thus, single micro and nanoelectrodes are ideal candidates for intercellular and extracellular electrochemical detection.^{30,31}

This body of work focusses on the fabrication, characterization, and application of gold and platinum micro and nanoelectrodes. The micro and nanoelectrodes were characterized by FE-SEM imaging and, electrochemically, using the redox probe ferrocene. The electrodes were then used to detect and determine silver at ultra-low concentrations (1 nM–80 nM) in chloride-free phosphate, pH 7.4. The electrochemical deposition and stripping analysis experiments were carried out in a three-electrode system using Ag/AgBr as a quasi-reference electrode. In all the electrochemical analysis performed, chlorides were

*Electrochemical Society Student Member.

^zE-mail: john.colleran@dit.ie

Table I. Literature summary of single micro and nanoelectrodes fabricated using the laser puller method (*nanopore formation and electrodeposition).

Electrode Material	Technique	Electrode Dimension	Application	Reference
Platinum	Glass puller and electrodeposition	60 nm	In vitro detection of ROS and RNS at the single-cell level	Christian Amatore ²⁷
Platinum and Gold	Laser puller and electrodeposition*	1–3 nm and 4 nm	Measure heterogeneous ET rates and electrocatalysis	Bo Zhang ^{32,33}
Platinum, carbon, gold, silver, and mercury	Laser puller	50 nm, 7 μm , 10 μm , 25 μm and 25 μm	SECM measurements	Janine Mazeroll ^{34,35}
Platinum	Laser Puller	2–500 nm	Kinetics of ET and SECM imaging of living cells	Michael V. Mirkin ^{36,37}
Platinum	Laser Puller	50–300 nm	Detect dilute electroactive species and dual electrodes	Peng Sun ^{38,39}
Platinum	Laser Puller	10 nm	SECM measurement	Wolfgang Schumann ⁴⁰
Gold	Laser Puller	5 nm	Electrochemistry of ferritin and E-DNA sensor	Yongxin Li ^{41,42}
Carbon fiber electrode	Micropipette puller	100 μm	Detection of H_2O_2	Leslie A. Sombers ⁴³
Platinum	Laser Puller	110 nm	ESD damage to nanoelectrodes	Shigeru Amemiya ⁴⁴

deliberately omitted, and meticulous electrode cleaning was implemented, resulting in the generation of reproducible calibration curves for silver detection at the gold and platinum micro and nanoelectrodes.

Experimental

Materials, chemicals, and instrumentation.—All chemicals were used as received from suppliers without further purification; silver nitrate (AgNO_3 – Sigma Aldrich, 99%), nitric acid (HNO_3 – Acros Organics, 60%), hydrobromic acid (HBr – Sigma Aldrich, ACS grade), potassium bromide (KBr – Riedel-de Haen, extra pure), monopotassium phosphate (KH_2PO_4 – Sigma Aldrich, ACS grade), dipotassium phosphate (K_2HPO_4 – Sigma Aldrich, ACS grade), potassium nitrate (KNO_3 – Merck, ISO grade), sodium nitrate (NaNO_3 – Sigma Aldrich, ACS grade), sulfuric acid (H_2SO_4 – Sigma Aldrich, 95–97%), acetonitrile (ACN – Riedel-de Haen, HPLC grade) and ferrocene ($(\text{Fe}(\text{C}_5\text{H}_5)_2)$ – Sigma Aldrich, 98%).

Quartz capillaries (O.D – 1.0 mm; I.D – 0.3 mm & 0.7 mm), and borosilicate capillaries (O.D – 1.0 mm; I.D – 0.3 mm) were purchased from Sutter Instruments. 25 μm diameter platinum wire (hard tempered) and gold wires (annealed) were purchased from Goodfellow and Alfa Aesar. Glass sealed gold microwires were generously donated by ELIRI, Moldova.

A Solartron potentiostat, model 1285, was used for experiments involving microelectrodes, while a CH Instruments potentiostat, model 620a, was used for nanoelectrode work. All electrochemical measurements were made using a three electrode system; gold and platinum micro, and nanoelectrodes were used as working electrodes, platinum wire as the counter electrode and Ag/AgBr as a quasi-reference electrode (silver detection), a nonaqueous Ag/Ag⁺ reference electrode (for ferrocene in acetonitrile, cyclic voltammetry) and a saturated calomel reference electrode (for aqueous cleaning of the electrodes). All electrochemical experiments were conducted at room temperature, in a homemade Faraday cage.

Chloride-Free phosphate buffer solution 0.1 M and 0.01 M (Chloride-free PB).—Chloride-free phosphate buffer was prepared using ultrapure water (18 $\text{M}\Omega\text{ cm}^{-1}$, Milli-Q) for 0.1 M PB (pH – 7.4) with salt concentration of 0.1 M KH_2PO_4 , 0.1 M K_2HPO_4 , 0.0027 M KNO_3 and 0.137 M NaNO_3 (only phosphate and nitrate salts were used). The 0.01 M chloride-free PB was prepared by further dilution of the stock 0.1 M chloride-free phosphate buffer (pH – 7.4) solution.

Silver nitrate.—A stock solution of 0.1 M silver nitrate was prepared and kept in the dark to protect it from light exposure. The working solutions were prepared by dilution of the stock solution for the desired concentration (1 nM – 1 μM).

Preparation of Ag/AgBr reference electrode.—When preparing the Ag/AgBr quasi-reference electrode, 1 M hydrobromic acid and 0.05 M potassium bromide were used for the bromination of silver wires. Galvanostatic deposition of bromide onto a silver wire was performed by applying a current of 10.16 mA to the wire for 1 hour in a solution of 1 M HBr. The bromidized silver wire was then soaked in 0.05 M potassium bromide for 3 hours.⁴⁵

Ferrocene.—1 mM ferrocene solutions were prepared by dissolving ferrocene in acetonitrile solution without supporting electrolyte.

Sulfuric acid.—Sulfuric acid solutions of 0.1 M, were prepared using ultrapure water (18 $\text{M}\Omega\text{ cm}^{-1}$, Milli-Q), and used for electrode cleaning.

Physical and electrochemical characterization.—A Hitachi SU-6600 FE-SEM and S5500 FE-SEM (Field Emission–Scanning Electron Microscopy) were used to acquire FE-SEM images in performing the physical and morphological characterization of the micro and nanoelectrodes. The samples were imaged as fabricated and no additional coating or sputtering was required.

Silver detection.—Anodic stripping voltammetry was employed to determine and quantify silver solution concentrations using micro and nanoelectrodes in chloride-free PB at pH 7.4. A detailed description on the optimization of electrochemical parameters for silver detection can be found in the Supplementary Materials (S4). The optimal deposition potential, –0.3 V, was applied to the electrodes for a duration of 1 minute, and for 30 seconds, for the micro and nanoelectrodes, respectively. The stripping experiments were repeated a minimum four times, and reproducible stripping charge (total charge transferred during the oxidation of silver at the electrode surface) values from the same electrode were obtained. The electrodes were cleaned by cycling the potential from –0.5 V to 1.5 V (nano) and –0.3 V to 1.2 V (micro) in 0.1 M sulfuric acid. Cycling was continued until the characteristic profiles for gold and platinum micro and nanoelectrodes were obtained. The cleaning procedure was continued and repeated until the silver stripping peak was no longer observed, when stripping voltammetry was performed in silver-free buffer. After each stripping analysis, the electrodes were cleaned by cycling in 0.1 M H_2SO_4 for 10 cycles. The silver stripping experiments were carried out at scan rates of 100 mV/s and 10 mV/s for the micro and nanoelectrodes, respectively.

Fabrication of microelectrodes and nanoelectrodes.—The microelectrodes were fabricated using a Sutter P-2000 laser puller and polished using a BV-10 beveler (Sutter Instruments). Quartz

capillaries were used for the fabrication of the micropipettes, with gold and platinum wires (25 μm diameter). Pre-cleaning is an essential step for the microelectrode fabrication process. The fabrication of the microelectrodes (Fig. 1a) involves three steps 1) micropipette fabrication, 2) heat sealing and, 3) polishing. Micropipettes were drawn using the laser puller, into which gold and platinum microwires were inserted and heat-sealed using a glow torch. Finally, the sealed microelectrodes were polished on the BV-10 beveler to expose the active metal surface by polishing the excess insulating pipette glass from the tip. Electrical connections were made by gluing thin copper wire to the Au and Pt wires in the electrodes using electrically conductive silver epoxy.

Pt microwires were inserted into quartz capillaries and the Pt wire-glass capillary assemblies were pre-thinned sealed, hard pulled and polished to fabricate platinum nanoelectrodes (Fig. 1b). The fabrication of gold nanoelectrodes, follows a different procedure from that of platinum nanoelectrodes, due to the difference in the melting points of gold (1064°C) and platinum (1768°C). A glass sealed gold microwire (ELIRI) was inserted into a borosilicate capillary to fabricate the gold nanoelectrodes. A detailed fabrication procedure for gold and platinum micro (S1), platinum (S2) and gold nanoelectrodes (S3) is given in the Supplementary Material.

Results and Discussion

Characterization of micro and nanoelectrodes.—The fabricated gold and platinum micro and nanoelectrodes were imaged using FE-SEM, which provides good evidence for the 2-D surface morphology. From Figure 2, a well-defined flat disk metal tip on the micro and nanoelectrodes can be observed. The radii of the gold and platinum microelectrodes, imaged by FE-SEM, were 17 and 10 μm , respectively (Figs. 2b and 2a). The gold and platinum nanoelectrode radii were 300 nm (polished further to reduce charging effect during SEM imaging) and 100 nm, respectively, are shown in Figure 2c and

Figure 2d. Steady-state voltammograms, obtained for ferrocene at the electrodes utilized for FE-SEM images, returned diffusion controlled steady-state currents of 75 pA and 87 pA for the gold and platinum nanoelectrodes, respectively (Figs. 3c and 3d). From these steady-state currents, the effective radii were calculated as 90 nm for the platinum and 73 nm for the gold nanoelectrodes.

The platinum microelectrode in Figure 2a was polished at an angle of 45° and 90° to evaluate the quality of polishing and to provide a smooth uniform flat circular electrode surface. In Figure 2b, the gold microelectrode of radius 17 μm reveals a proper concentric sealing of the gold wire within the insulating glass capillary. The gold nanoelectrode, shown in Figure 2c, presents outer and inner glass capillaries encasing the gold wire. A 100 nm radius platinum nanoelectrode is shown in Figure 2d and Figure 2e, (Fig. 2e was imaged using low-angle backscattering). Figure 2f (insert: nanoelectrode tip with tapered and untapered regions) shows a platinum nanoelectrode tip radius of 30 nm.

The ferrocene/ferrocenium (Fc/Fc^+) couple is an excellent redox probe (1 mM) in acetonitrile to investigate the electrochemical properties of the fabricated electrodes. The cyclic voltammetric behavior of the micro and nanoelectrodes were recorded without added supporting electrolyte.^{40,46} The FE-SEM images confirm the integrity of the electrodes and that the geometry of each micro and nanoelectrode active surface is flat and disk-shaped.

From the voltammetry experiments, the micro and nanoelectrodes exhibit ideal current sigmoidal profiles, with no hysteresis on the reverse scans (Fig. 3). The negligible current variations in the plateau region of the profiles, Figures 4c and 4d, for the gold and platinum nanoelectrodes, were of the order of picoamperes at a scan rate of 50 mV/s. These picoamp current spikes may be due to ohmic resistance or overlay capacitance, which is known to occur at electrodes characterized in the absence of supporting electrolyte.^{41,46} The radius of each electrode was calculated from the diffusion limited steady-state current response in 1 mM ferrocene for the disk-shaped electrodes

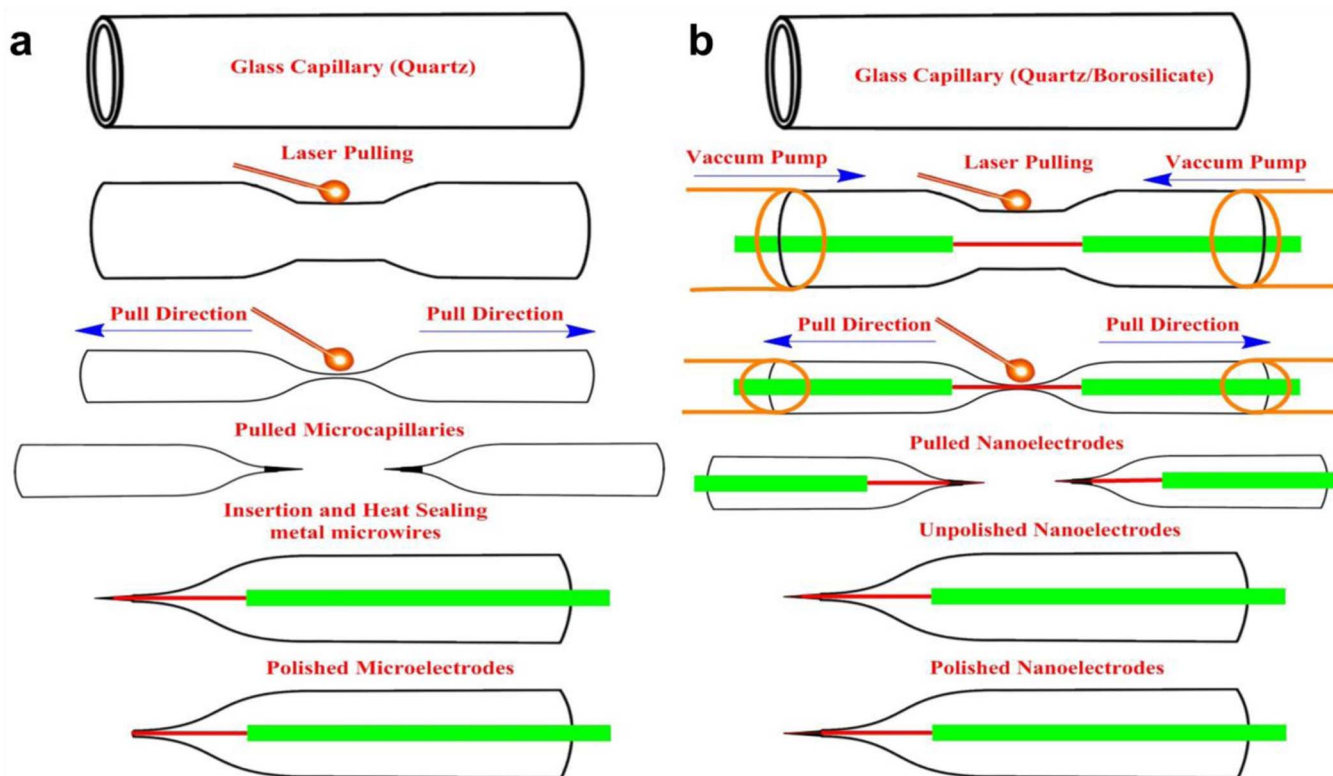


Figure 1. Graphical representation of laser pulled fabrication process for a) both gold and platinum microelectrodes and b) platinum nanoelectrodes. Capillaries loaded with gold and platinum microwires were laser pulled forming the microelectrodes. For nanoelectrode fabrication, laser pulled heat-sealed capillaries were used.

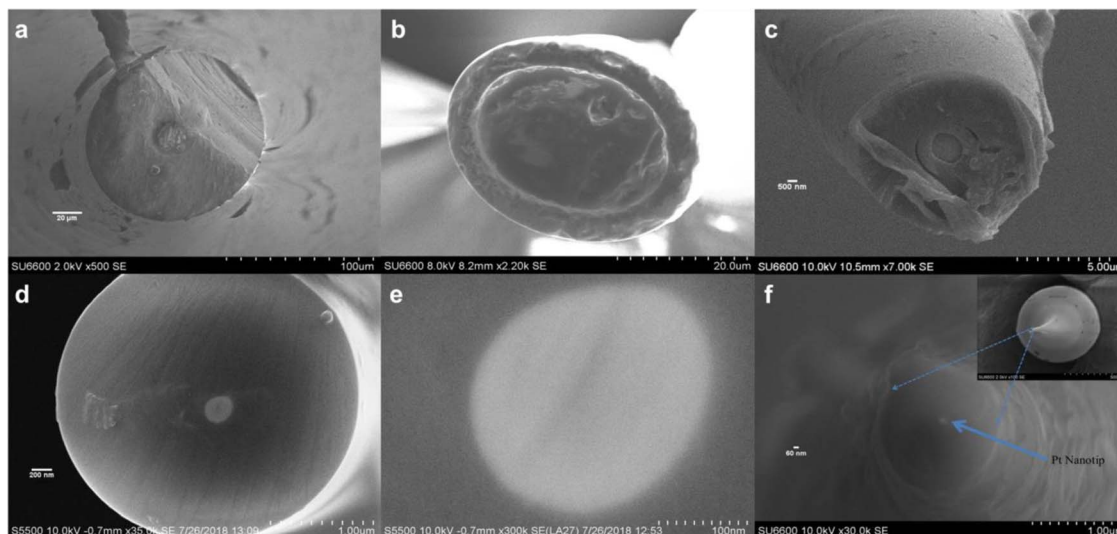


Figure 2. SEM images showing the surface morphology of the electrode tips; a) platinum microelectrode (10 μm) polished at an angle of 45° and 90°, showcasing the smoothness of electrode polishing; b) gold microelectrode (17 μm); c) gold nanoelectrode (outer and inner glass capillary encasing the gold wire); d) platinum nanoelectrode of 100 nm radius and e) imaged using low-angle backscattering; f) platinum nanoelectrode tip of 30 nm in radius (insert: nanoelectrode tip showing tapered and untapered regions).

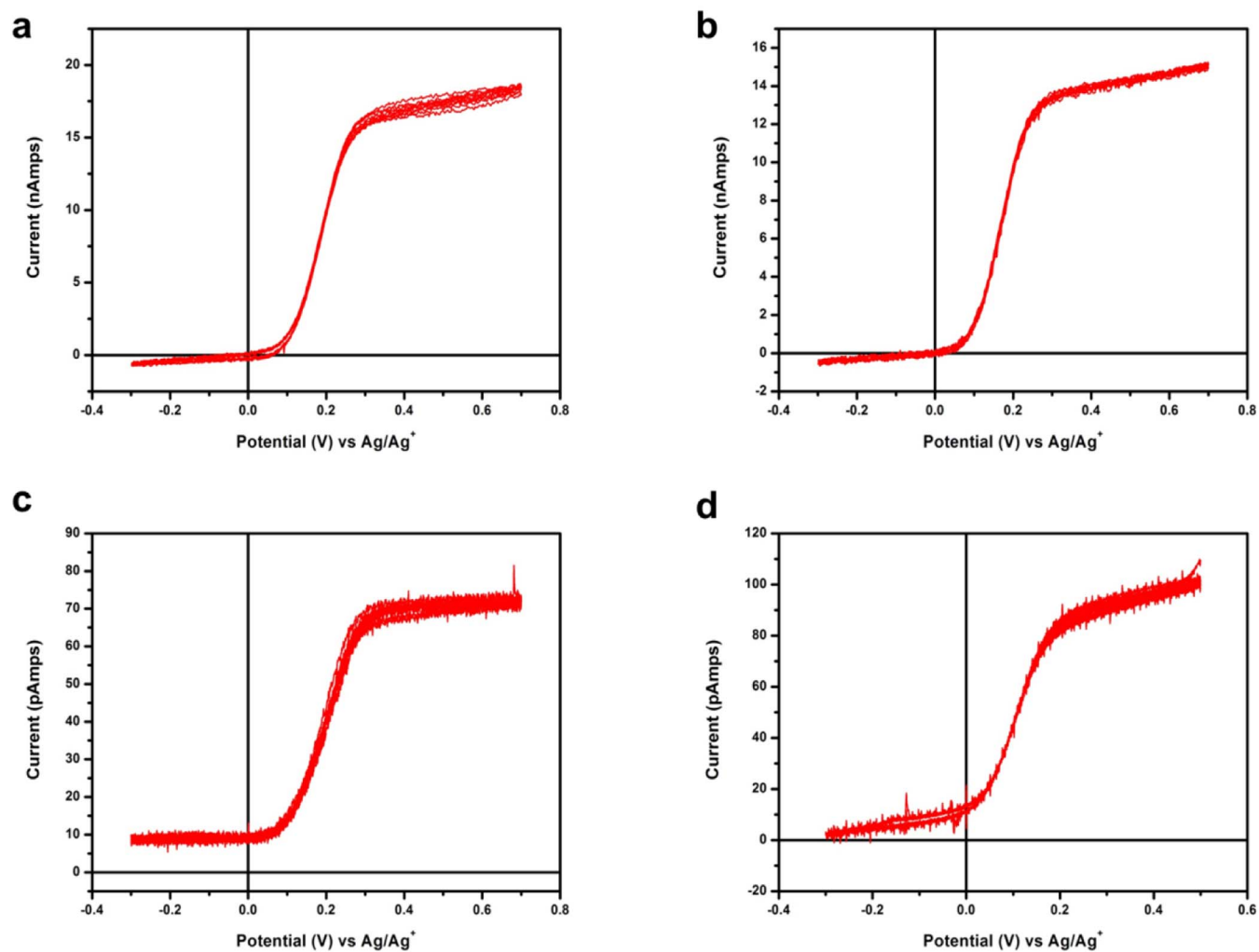


Figure 3. Cyclic voltammetry of 1 mM ferrocene in acetonitrile without added supporting electrolyte at a) a) gold microelectrode ($r \sim 20 \mu\text{m}$); b) platinum microelectrode ($r \sim 15 \mu\text{m}$); c) gold nanoelectrode ($r \sim 73 \text{ nm}$); d) platinum nanoelectrode (radius 90 nm). The unsmoothed CV's of gold and platinum microelectrodes were obtained at 20 mV/s and nanoelectrodes at 10 mV/s scan rates for 5 cycles.

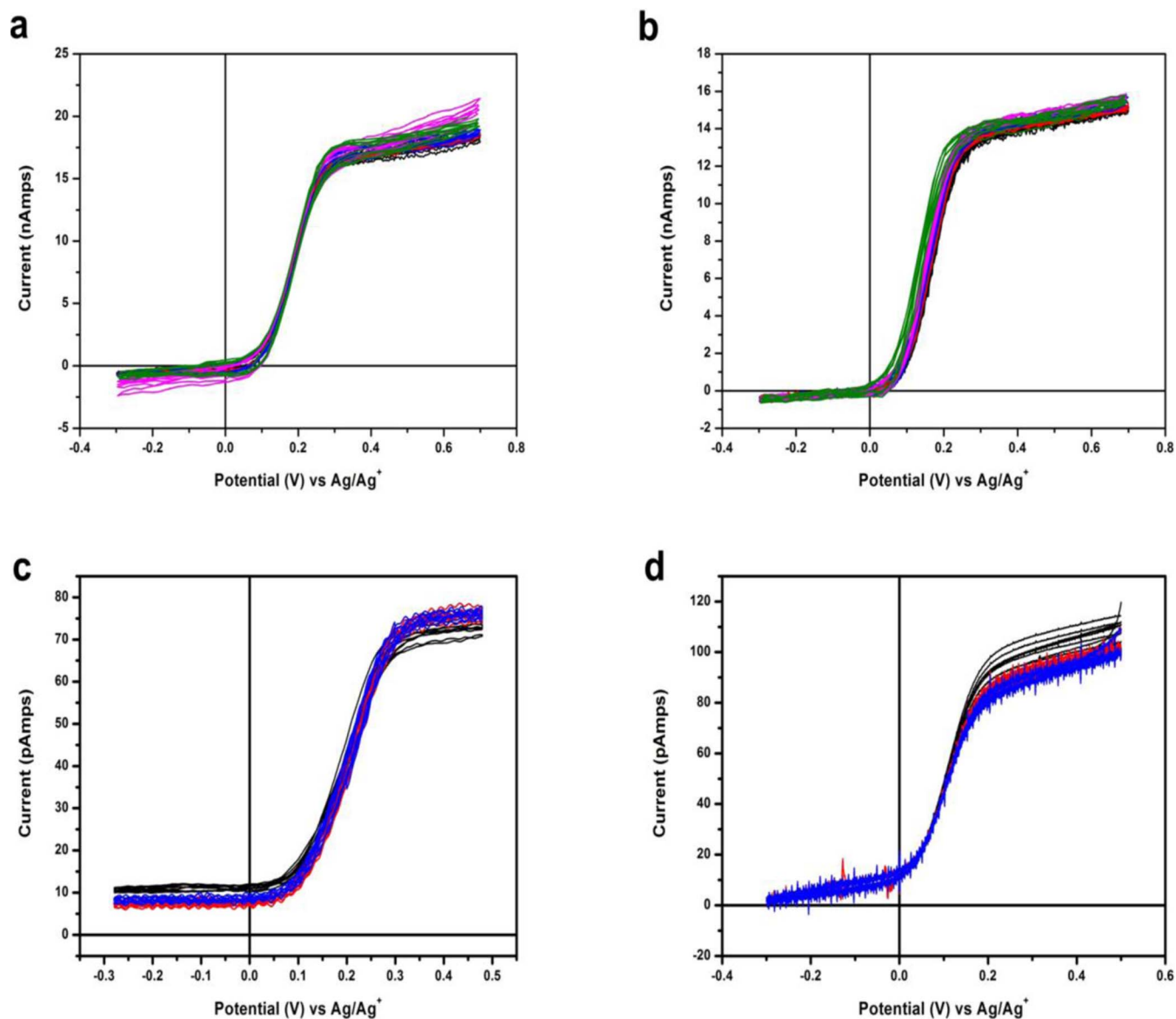


Figure 4. Cyclic voltammetric performance of fabricated electrodes in ferrocene, in the absence of supporting electrolyte, at different scan rates; a) at gold ($r \sim 20 \mu\text{m}$) and b) platinum microelectrodes ($r \sim 15 \mu\text{m}$), at 20 (black), 50 (red), 100 (blue), 150 (green) and 200 mV/s (pink); c) at gold ($r \sim 73 \text{ nm}$) and d) platinum nanoelectrodes ($r \sim 90 \text{ nm}$), at 10 (black), 20 (red) and 50 mV/s (blue).

using the following equation:³²

$$i_{ss} = 4nFDC_b a$$

where n is the number of electrons transferred per molecule, F is the Faraday constant (96,485 C/mol), D is the diffusion coefficient of ferrocene in acetonitrile ($2.3 \times 10^{-5} \text{ cm}^2/\text{s}$),⁴⁷ C_b is the bulk concentration of ferrocene (mol/cm^3) and a is the radius of the electrode.

The radii of the nano and microelectrodes were calculated to be in the ranges 100–150 nm (radii between of 1–10 nm for gold and platinum nanoelectrodes, Fig S5 and Fig S6 in the Supplementary Material) and 15–20 μm , respectively, using the diffusion controlled steady-state currents. Cyclic voltammetry of the Fc/Fc^+ redox couple confirm the dimensions observed in the FE-SEM images. These data provide evidence that good quality flat disk-shaped, leak-free non-recessed electroactive micro and nanoelectrodes were fabricated. The sigmoidal-shaped voltammograms exhibiting steady-state limiting current profiles, prove that a good seal and quality polished electrodes were produced.^{34,48} Since the cyclic voltammetry current profiles are independent of applied scan rate (Fig. 4), theory indicates

that the electrodes are highly stable and are leak/crack free and, thus, exhibit excellent electrochemical performance.⁴¹

Nanomole silver detection in chloride-free phosphate Buffer, pH 7.4.—Silver detection experiments were carried out at a platinum macroelectrode in a 1 μM solution of silver nitrate in chloride-free PB (pH = 7.4) to identify the optimal potentials for silver deposition and stripping analysis (Fig. 5). The optimization of the electrochemical conditions was carried out for deposition potential, deposition time, electrolyte, pH, scan rate and buffer concentration (Supplementary Materials, S4).

The cyclic voltammetry profile features a reduction peak at -0.3 V (Ag^+ to Ag^0) and a corresponding stripping peak oxidation potential at 0.32 V (Ag^0 to Ag^+). Silver concentrations, ranging from 1–80 nM in chloride-free PB, were investigated using the following optimized conditions; deposition potential -0.3 V vs Ag/AgBr was applied for 60 seconds and 30 seconds, and stripped at 10 and 100 mV/s for the micro and nanoelectrodes, respectively. The cyclic voltammetry data for a 1 μM silver nitrate solution were collected using both saturated

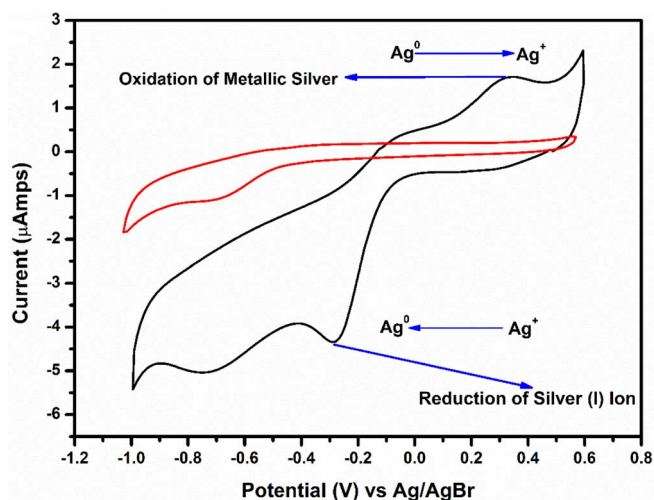


Figure 5. Cyclic voltammetry of $1 \mu\text{M}$ concentration of AgNO_3 in chloride-free PB at a gold macroelectrode against Ag/AgBr (black) and blank chloride-free PB (red). The oxidation of silver was observed at a potential of 0.32 V and a reduction peak at -0.3 V and reduction of dissolved O_2 at -0.75 V . Scan rate was 100 mV/s .

calomel and an Ag/AgBr quasi-reference electrodes. Results reveal that the Ag/AgBr quasi-reference electrode is a more suitable reference electrode for silver detection experiments.

In this work, the working electrodes were cleaned by cycling in 0.1 M sulfuric acid until reproducible characteristic profiles were obtained (Fig S7 in the Supplementary Material). As reported in the literature, thorough electrode cleaning enhances the reproducibility of the stripping analysis. The higher the renewable surface available for deposition, the greater the reproducibility obtained.^{49,50} The background correction of stripping peaks (Fig. 6) allows quantification of the total stripping charge during the oxidation of silver even for short deposition times and at ultra-low concentrations (nanoelectrode – 30 seconds deposition).⁵⁰ The percentage error in the background correction, decreased when the optimal deposition potential -0.3 V and deposition duration were used.¹⁹ It has been reported that calibration curves generated using charge instead of peak current have higher correlation coefficients for silver detection.⁵¹

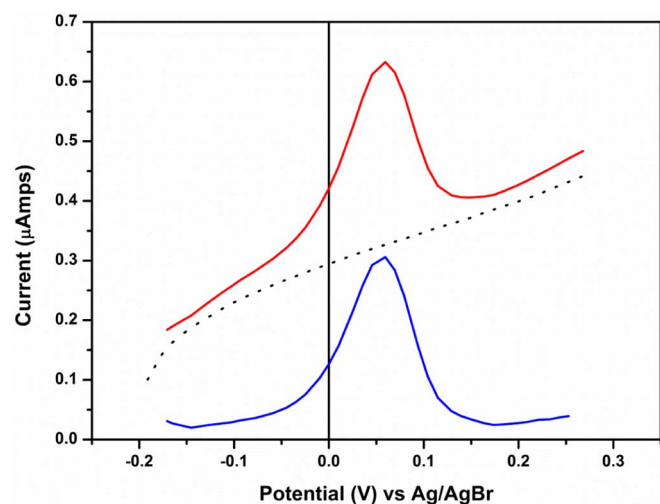


Figure 6. Typical experimental stripping peak subtraction (red) using the background profile (dotted), and the subtracted peak (blue), was used to calculate the peak charge. The stripping peak of silver ($1 \mu\text{M}$) in chloride-free PB in 10 mV/s scan rate at platinum microelectrode ($r \sim 10 \mu\text{m}$).

Chloride-free phosphate buffer solution was used in this work, in order to eliminate the formation of silver chloride precipitates ($\text{Ag}^+ \text{Cl}^-$ complexation is in the order of 10^{-9} M) and to obtain reproducible stripping charge values for silver concentrations as low as 1 nM . Further contamination of chloride was eliminated by replacing the saturated calomel reference electrode with an Ag/AgBr quasi-reference electrode. The effect of chloride ions on the stripping of silver was studied by analysing the anodic stripping peak in the presence and absence of chloride ions. It was found that in the presence of chloride, there is a shift in the anodic stripping peak to less positive potential values and an additional stripping peak is observed (Fig. 7a).⁵² From Figure 7a, this doublet of silver stripping peaks arise at 0.05 V and -0.05 V vs SCE. The oxidation potential of metallic silver is 0.05 V and the peak in the negative potential (-0.05 V) can be attributed to the oxidation of deposited silver chloride at the electrode surface.⁵² In contrast, experiments performed when using a Ag/AgBr reference electrode return a single well-defined stripping peak profile (Fig. 7b).

In 0.1 M phosphate buffer, the chloride concentration is 0.137 M , and, to maintain equivalent ionic strength, nitrate ions of the same concentration were used for 0.1 M chloride-free phosphate buffer. The presence of chloride ions in high concentration (0.137 M) results in poor reproducibility of silver stripping analysis, resulting in a narrowing of the stripping peak, reportedly due to the formation of insoluble silver chloride nanoparticles.^{22,23,53} Epple et al., reported that silver in biological buffers tends to precipitate as silver chloride nanoparticles and AgCl colloids, which are toxic to cells. The authors also reported that in PBS (chloride present) silver chloride nanoparticles, ranging between $500\text{--}1000 \text{ nm}$ in diameter, form in solution.⁵⁴ The concentration gradient of silver and silver chloride nanoparticles at the electrode-electrolyte interface greatly impacts on the reproducibility of silver anodic stripping profiles. In this work, a single stripping peak (Fig. 7b) indicates that there is no formation of AgCl and that monolayer deposition of metallic silver occurs at the micro and nano electrode surfaces.⁵⁵

The stripping experiments were conducted at platinum nanoelectrodes with, initially, different concentrations of phosphate ions in 0.1 M and 0.01 M chloride-free PB, pH 7.4 (Fig. 8), as bio-electrochemical experiments have been carried out in both concentrations.⁵⁶ The stripping peaks obtained in 0.1 M PB solution were much sharper than those obtained in 0.01 M PB, and the charges transferred during the oxidation of silver in 0.01 M PB were less than the charges recorded in 0.1 M PB. The extreme differences in stripping currents may be solely due to the difference of ionic strength of both buffer solutions.⁵⁷ However, phosphate ions present in PB solution, specifically the dibasic anion (HPO_4^{2-}), are reported to greatly influence the dynamics of silver oxidation, which might also contribute to the differences in the charge observed.⁵⁸ It was found that a 94.33% decrease in current values (i_{pmax}) for the oxidation of silver in 0.01 M chloride-free PB was recorded, when compared to the 0.1 M medium, at a platinum nanoelectrodes (Fig. 8). In addition, silver concentrations of 20 nM or less, returned statistically equal stripping peak currents at the platinum nanoelectrodes. Thus, for the silver detection studies presented here, due to excellent reproducibility, a 0.1 M buffer concentration was utilized. In both chloride-free phosphate buffer concentrations at pH 7.4, there was no silver chloride formation, thus, there were no impurities present to influence the diffusion coefficient of silver ions or the rate constant for silver oxidation.⁵²

Detailed reviews of the literature for the determination of ultra-low concentrations of silver at carbon electrodes have been reported, and provide an insight into electrolytes used (HNO_3 , acetate buffer, KCl and NH_4NO_3) and pH range ($1\text{--}5.5$).^{11,15,59} These data indicate that silver oxidation is pH-dependant.⁶⁰ The linearity of each calibration plot increased as the size of the electrode decreased for lower concentrations of silver, and can be attributed to the enhanced electrochemical properties of nanoelectrodes compared to conventional electrodes. Mass transfer at micro and nanoelectrodes is governed by radial diffusion which promotes the deposition of silver on the surface, thus, enhances the sensitivity of the electrode. A non-zero intercept

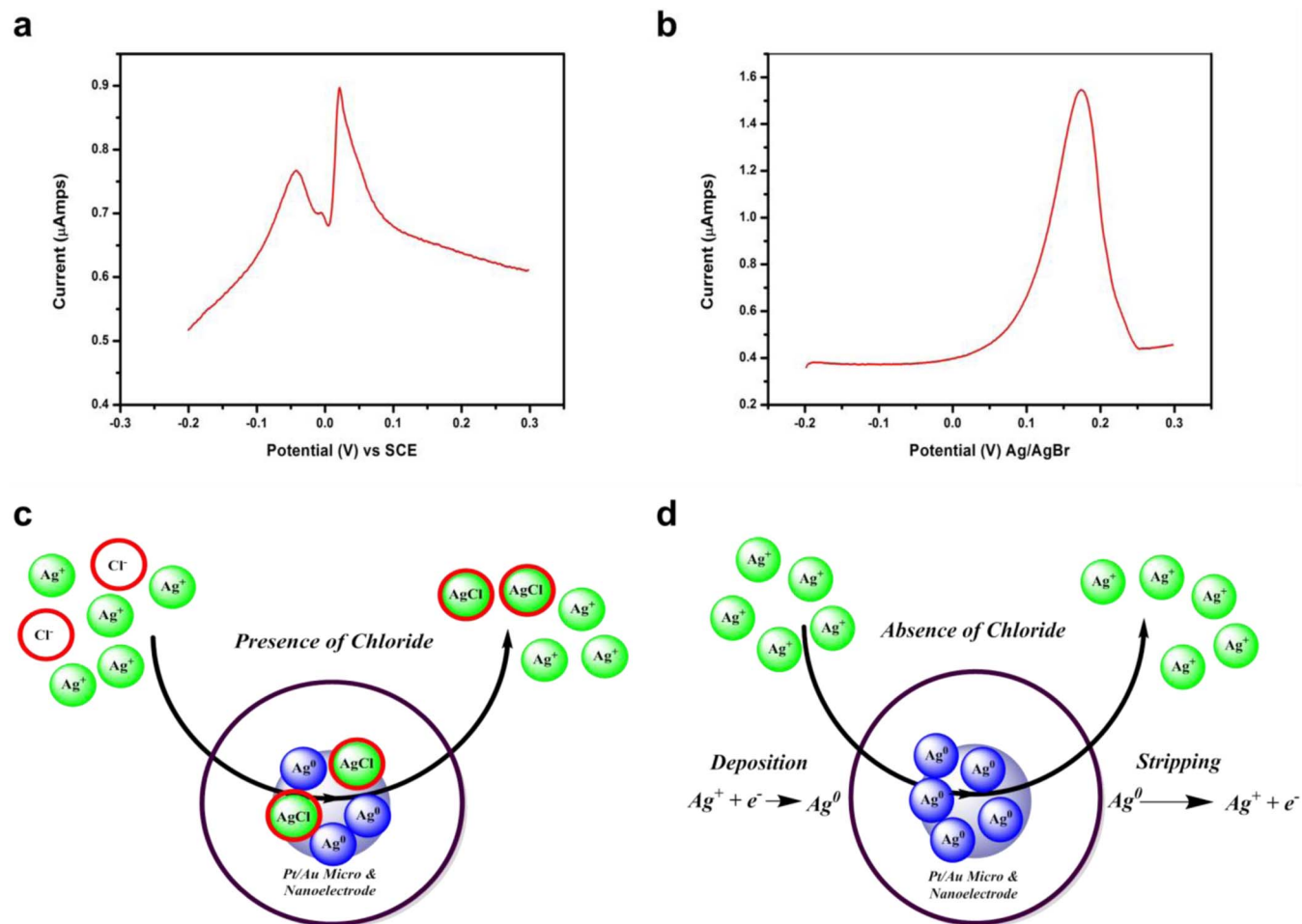


Figure 7. Stripping peak of 1 μM concentration of silver at deposition duration – 1 min; deposition potential –0.3 V, scan rate 10 mV/s; a) PB containing chloride (0.137 M) vs SCE reference electrode (multiple peaks at 0.05 V for oxidation of Ag to Ag⁺ and –0.05 V for oxidation of Ag to AgCl); b) chloride-free PB solution vs Ag/AgBr reference electrode (single silver oxidation peak at 0.18 V). Graphical representation of the influence of chloride in silver detection, c) in the presence and d) in the absence of chloride.

was observed in the regression plots for both micro and nanoelectrodes (Fig. 9). The average charge values, with standard deviation, from 0.01 M and 0.1 M chloride-free phosphate buffer, for micro and

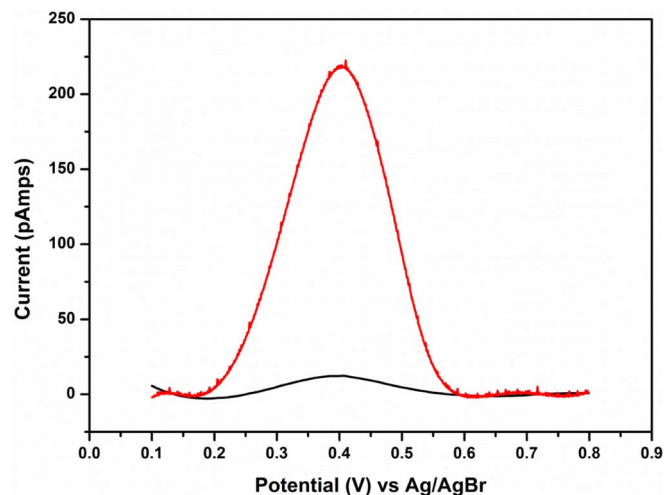


Figure 8. Comparison of the stripping peak for 80 nM concentration of silver performed in 0.01 M (black) and 0.1 M (red) in chloride-free PB, at a scan rate of 10 mV/s obtained, at platinum nanoelectrode (90 nm).

nanoelectrodes of platinum and gold, are summarized in Tables II and III.

The stripping charges were calculated and plotted against silver concentrations to construct calibration curves. Using the linear regression model, the data signify that the micro and nanoelectrodes exhibit excellent stability and reproducibility, returning linear ranges for silver concentrations of 1–80 nM in chloride-free PB at pH 7.4. Thus, platinum and gold nanoelectrodes were deemed suitable for the detection and quantification of ultra-low concentrations of silver (Fig. 10).

Radulescu et al., studied the influence of acetate buffer (pH – 5.2), citrate buffer (pH – 3.0) and PBS (chloride present, pH – 7.0) on the determination of silver by DPV. The authors concluded that only acetate buffer, pH 5.2, is a suitable medium for silver stripping analysis with a limit of detection (LoD) of 25 nM. Real tap water samples were used for analysis, and the electrodes returned 96–106% recovery of silver ions.¹⁴ Carbon paste electrodes modified with a nanosized silver imprinted polymer, were used for nanomolar silver detection in the water samples (pH 2, acidified with HNO₃) and acetate buffer (pH 5). The author's reported a 0.12 nM limit of detection and a recovery of 97.7–101.3% in tap, river and ground water samples.¹² Detection of silver in water samples (pH 1.1, addition of HNO₃ and KCl) using graphite felt electrodes with DVP experiments, returned a LoD of 25 nM.²¹ Recent work reported the detection of silver nanoparticles in real samples (bottled and tap water), with a low detection concentration of 12 pM, using particle impact electrochemistry.^{61,62} In this work, excellent reproducibility was obtained for 1–80 nM

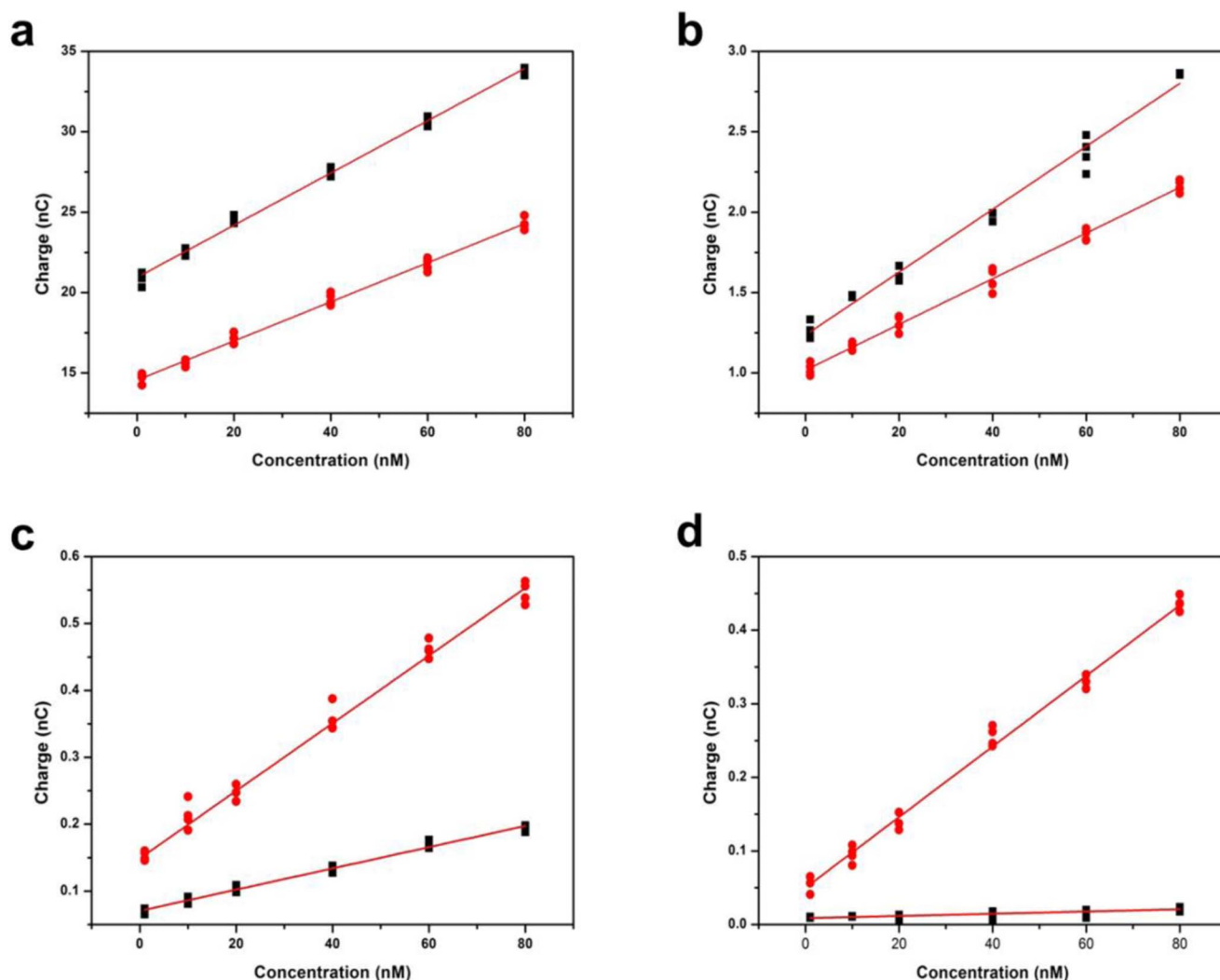


Figure 9. Linear regression plot for 0.01 M (black squares) and 0.1 M (red circles) PB (pH 7.4) at a) a gold microelectrode ($r \sim 20 \mu\text{m}$), b) a platinum microelectrode ($r \sim 15 \mu\text{m}$), c) a gold nanoelectrode ($r \sim 73 \text{ nm}$), and d) a platinum nanoelectrode (60 nm). Silver concentrations range from 1 nM to 80 nM. Each plot represents four independent sets of experimental data obtained at the same nanoelectrodes. The average values and standard deviation ($n = 3$) are given in Tables II and III.

concentrations, with a limit of detection (LoD) of 1.3 pM ($S/N - 3.1$), and relative standard deviation of 1.8% (RSD for 10 nM) for silver detection in 0.1 M chloride-free phosphate buffer at platinum nanoelectrodes. In this work, the fabricated platinum microelectrodes were employed to detect silver from spiked samples in 0.1 M chloride-free phosphate buffer (summarized in Table IV). The analytical results for the recovery analysis of silver were between 95.4%–98.6%. These recovery values in 0.1 M chloride-free phosphate buffer indicates suc-

cessful application of the fabricated micro and nanoelectrodes for the electrochemical detection of silver.

Conclusions

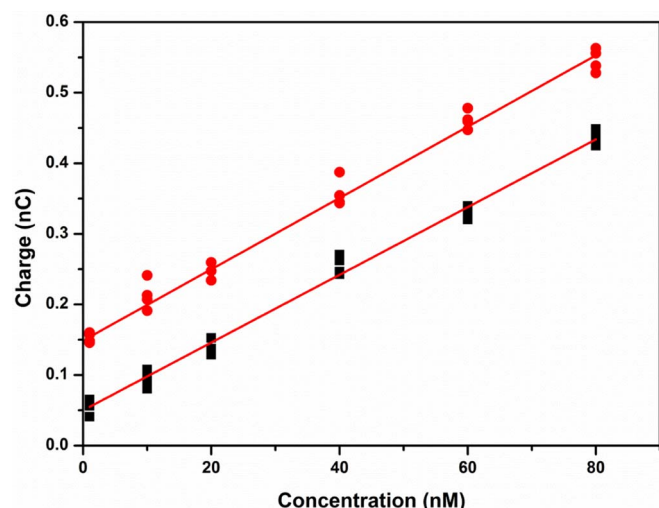
To conclude, in this body of work, the electrochemical detection and determination of silver in chloride-free PB, pH 7.4, is presented. Micro and nanoelectrodes of gold and platinum, fabricated using the

Table II. The average charge values and standard deviation ($n = 3$) for 0.01 M and 0.1 M chloride-free phosphate buffer for platinum and gold microelectrodes.

Concentration, nM	Average Charge, nC			
	0.01M		0.1 M	
	Platinum	Gold	Platinum	Gold
1	1.266 ± 0.049	20.890 ± 0.404	1.024 ± 0.037	14.696 ± 0.315
10	1.478 ± 0.009	22.504 ± 0.253	1.168 ± 0.021	15.605 ± 0.183
20	1.613 ± 0.048	24.620 ± 0.270	1.308 ± 0.050	17.081 ± 0.347
40	1.968 ± 0.036	27.446 ± 0.254	1.581 ± 0.072	19.598 ± 0.375
60	2.366 ± 0.102	30.717 ± 0.275	1.857 ± 0.035	21.729 ± 0.395
80	2.859 ± 0.005	33.789 ± 0.260	2.162 ± 0.037	24.285 ± 0.370

Table III. The average charge values and standard deviation ($n = 3$) for 0.01 M and 0.1 M chloride-free phosphate buffer for platinum and gold nanoelectrodes.

Concentration, nM	Average Charge, nC			
	0.01M		0.1 M	
	Platinum	Gold	Platinum	Gold
1	0.0095 ± 0.0006	0.071 ± 0.004	0.056 ± 0.011	0.152 ± 0.007
10	0.010 ± 0.0004	0.087 ± 0.005	0.095 ± 0.011	0.213 ± 0.002
20	0.011 ± 0.0009	0.101 ± 0.006	0.139 ± 0.012	0.227 ± 0.013
40	0.014 ± 0.0006	0.132 ± 0.007	0.255 ± 0.013	0.357 ± 0.020
60	0.017 ± 0.0005	0.170 ± 0.006	0.327 ± 0.009	0.461 ± 0.012
80	0.022 ± 0.003	0.193 ± 0.005	0.436 ± 0.009	0.546 ± 0.016

**Figure 10.** Comparison of calibration curves for platinum (black squares) and gold nanoelectrodes (red circles) in 0.1 M chloride-free phosphate buffer (deposition duration 30 seconds and potential -0.3 V vs Ag/AgBr containing 1–80 nM of AgNO_3). For each concentration, at least four independent sets of experimental data at the same nanoelectrode were obtained. The R-square value from the calibration curves indicates that platinum nanoelectrodes ($R^2 = 0.992$) and gold nanoelectrodes ($R^2 = 0.974$) are suitable substrates for silver detection in chloride-free phosphate buffer, pH 7.4.

laser puller method, exhibit good quality sealing and stability as characterized by FE-SEM and the redox probe ferrocene. We have demonstrated that by using the optimized laser pulling parameters for gold and platinum, robust micro and nanoelectrodes can be successfully fabricated. The fabricated micro and nanoelectrodes were utilized in the determination of ultra-low concentrations of silver in chloride-free PB, pH 7.4, yielding highly reproducible results. This study also briefly explored the effect of chloride and phosphate ions on silver sensing. Eliminating chloride ions and using a Ag/AgBr quasi-reference electrode, provides an excellent system for the detection of nano and possibly sub-nanomolar concentrations of silver. This work will provide

Table IV. Recovery results for spiked silver concentrations in 0.1 M chloride-free phosphate buffer at a platinum microelectrode. Each plot represents four independent ($n = 3 \pm \text{SD}$) sets of experimental data (background corrected) obtained at the same microelectrode.

Sample	Added (nM)	Found (nM)	Recovery (%)
		Platinum	Platinum
0.1 M Chloride-free phosphate buffer (pH 7.4)	40	38.16 ± 0.02	95.4
	60	58.37 ± 0.01	97.3
	80	78.88 ± 0.01	98.6

a platform to probe into the mechanism of action of silver-based drugs via electrochemical speciation studies, in cell sustaining chloride-free phosphate buffer for in vitro and, potentially, in vivo conditions.

Acknowledgments

The work was performed in the Applied Electrochemistry Group (AEG), FOCAS Research Institute, Technological University Dublin, funded through the Fiosraigh Dean of Graduate Research School Award. We thank, Dr Brain Gorey, FOCAS, Dublin Institute of Technology for some of the FE-SEM images. FE-SEM imaging was also carried out at the Nano Research Facility in Dublin City University, funded through the Programme for Research in Third Level Institutions (PRTL), Cycle 5. We would also like to thank, ELIRI, Moldova, for generously donating the glass-sealed gold microwires for fabrication of the gold nanoelectrodes.

ORCID

Prabhakar Sidamaram <https://orcid.org/0000-0002-5430-7935>
John Collieran <https://orcid.org/0000-0001-5694-9010>

References

- S. P. Fricker, *Dalt. Trans.*, 4903 (2007).
- U. Ndagi, N. Mhlongo, and M. E. Soliman, *Drug Des. Devel. Ther.*, **11**, 599 (2017).
- M. Frezza, S. Hindo, D. Chen, A. Davenport, S. Schmitt, D. Tomco, and Q. P. Dou, *Curr. Pharm. Des.*, **16**, 1813 (2010).
- S. H. Van Rijt and P. J. Sadler, *Drug Discov. Today*, **14**, 1089 (2010).
- C. N. Banti and S. K. Hadjikakou, *Metalomics*, **5**, 569 (2013).
- L. Thornton, V. Dixit, L. O. N. Assad, T. P. Ribeiro, D. D. Queiroz, A. Kellett, A. Casey, J. Collieran, M. D. Pereira, G. Rochford, M. McCann, D. O'Shea, R. Dempsey, S. McClean, A. F. A. Kia, M. Walsh, B. Creaven, O. Howe, and M. Devereux, *J. Inorg. Biochem.*, **159**, 120 (2016).
- B. Biersack, A. Ahmad, F. H. Sarkar, and R. Schobert, *Curr. Med. Chem.*, **19**, 3949 (2012).
- S. Chernousova and M. Epple, *Angew. Chemie - Int. Ed.*, **52**, 1636 (2013).
- K. B. Holt and A. J. Bard, *Biochemistry*, **44**, 13214 (2005).
- J. P. Guggenbichler, M. Bösward, S. Lugauer, and T. Krall, *Infection*, **27**, S16 (1999).
- T. J. Davies, *Analyst*, **141**, 4742 (2016).
- R. Zhiani, M. Ghanei-Motlag, and I. Razavipanah, *J. Mol. Liq.*, **219**, 554 (2016).
- L. Liu, C. Wang, and G. Wang, *Anal. Methods*, **5**, 5812 (2013).
- M. C. Radulescu, A. Chira, M. Radulescu, B. Bucur, M. P. Bucur, and G. L. Radu, *Sensors*, **10**, 11340 (2010).
- R. Mikelova, J. Baloun, J. Petrova, V. Adam, L. Havel, J. Petrek, A. Horna, and R. Kizek, *Bioelectrochemistry*, **70**, 508 (2007).
- S. P. Perone, *Anal. Chem.*, **35**, 2091 (1963).
- B. K. Bansod, T. Kumar, R. Thakur, S. Rana, and I. Singh, *Biosens. Bioelectron.*, **94**, 443 (2017).
- A. R. Nisbet and A. J. Bard, *J. Electroanal. Chem.*, **6**, 332 (1963).
- J. Wang and B. Greene, *Anal. Chim. Acta*, **144**, 137 (1982).
- D. Dospivova, D. Hynek, L. Trmkova, and J. Hubalek, in *Setkání fyzikálních chemiků a elektrochemiků, Květen*, 2012, pp. 3.
- T. J. Davies, *Analyst*, **141**, 4742 (2016).
- S. yudong wang Dong, *Anal. Chim. Acta*, **212**, 341 (1988).
- D. E. Schildkraut, P. T. Dao, J. P. Twist, A. T. Davis, and K. A. Robillard, *Environ. Toxicol. Chem.*, **17**, 642 (1998).
- M. Li, H. Gou, I. Al-Ogaidi, and N. Wu, *ACS Sustain. Chem. Eng.*, **1**, 713 (2013).
- Y. Wu and S. Hu, *Indian J. Chem. - Sect. A Inorganic, Phys. Theor. Anal. Chem.*, **44**, 891 (2005).

26. A. J. Wain, eds. J. D. Wadhawan and R. G. Compton, Royal Society of Chemistry, Cambridge, 2013, vol. **12**, pp. 44.
27. Y. Wang, J.-M. Noël, J. Velmurugan, W. Nogala, M. V. Mirkin, C. Lu, M. Guille Collignon, F. Lemaître, and C. Amatore, *Proc. Natl. Acad. Sci. U. S. A.*, **109**, 11534 (2012).
28. I. W. Donald and B. L. Metcalfe, *J. Mater. Sci.*, **31**, 1139 (1996).
29. D. W. M. Arrigan, *Analyst*, **129**, 1157 (2004).
30. J. Clausmeyer and W. Schuhmann, *TrAC - Trends Anal. Chem.*, **79**, 46 (2016).
31. P. Actis, S. Tokar, J. Clausmeyer, B. Babakinejad, S. Mikhaleva, R. Cornut, P. Novak, A. I. Shevchuck, J. A. Dougan, W. Schuhmann, D. Klenerman, O. D. A. Rusakov, E. V. Sviderskaya, and Y. E. Korchev, *ACS Nano*, 875 (2014).
32. B. K. Jena, S. J. Percival, and B. Zhang, *Anal. Chem.*, **82**, 6737 (2010).
33. Y. Li, D. Bergman, and B. Zhang, *Anal. Chem.*, **81**, 5496 (2009).
34. L. Danis, D. Polcari, A. Kwan, S. M. Gateman, and J. Mauzeroll, *Anal. Chem.*, **87**, 2565 (2015).
35. M. A. Mezour, M. Morin, and J. Mauzeroll, *Anal. Chem.*, **83**, 2378 (2011).
36. Y. Shao, M. V. Mirkin, G. Fish, S. Kokotov, D. Palanker, and A. Lewis, *Anal. Chem.*, **69**, 1627 (1997).
37. B. Liu, S. Rotenberg, and M. Mirkin, *Anal. Chem.*, **74**, 6340 (2002).
38. C. Yang and P. Sun, *Anal. Chem.*, **81**, 7496 (2009).
39. P. Sun, J. Kitt, N. Tran, J. Dang, D. P. Saavedra, J. Hong, R. Wampler, and S. Anz, *Electroanalysis*, **28**, 1880 (2016).
40. B. B. Katemann and W. Schuhmann, *Electroanalysis*, **14**, 22 (2002).
41. Y. Zhang, S. Xu, Y. Qian, X. Yang, and Y. Li, *RSC Adv.*, **5**, 77248 (2015).
42. Y. Zhang, S. Xu, X. Xiao, Y. Liu, Y. Qian, and Y. Li, *Chem. Commun.*, **53**, 2850 (2017).
43. A. L. Sanford, S. W. Morton, K. L. Whitehouse, H. M. Oara, L. Z. Lugo-Morales, J. G. Roberts, and L. A. Sombers, *Anal. Chem.*, **82**, 5205 (2010).
44. N. Nioradze, R. Chen, J. Kim, M. Shen, P. Santhosh, and S. Amemiya, *Anal. Chem.*, **85**, 6198 (2013).
45. J. K. Taylor and E. R. Smith, *Natl. Bur. Stand.*, **22**, 307 (1939).
46. A. M. Bond and P. A. Lay, *J. Electroanal. Chem. Interfacial Electrochem.*, **199**, 285 (1986).
47. A. J. Bard and L. R. Faulkner, *Electrochemical Methods: Fundamentals and Applications, 2nd Edition*, 2000.
48. Y. Li, Q. Wu, S. Jiao, C. Xu, and L. Wang, *Anal. Chem.*, **85**, 4135 (2013).
49. S.-S. Hunag, *Analyst*, **119**, 1859 (1994).
50. J. Wang, R. Li, and H. Huiliang, *Electroanalysis*, **1**, 417 (1989).
51. J. Goł and J. Osteryoung, *Anal. Chim. Acta*, **181**, 211 (1986).
52. H. S. Toh, C. Batchelor-Mcauley, K. Tschulik, and R. G. Compton, *Analyst*, **138**, 4292 (2013).
53. S. Dong, *Anal. Chim. Acta*, **199**, 167 (1987).
54. K. Loza, C. Sengstock, S. Chernousova, M. Köller, and M. Epple, *RSC Adv.*, **4**, 35290 (2014).
55. U. R. I. Eisner and H. B. Mark, *J. Electroanal. Chem. Interfacial Electrochem.*, **24**, 345 (1970).
56. Z. Xie, J. Huang, S. Luo, Z. Xie, L. Xie, J. Liu, Y. Pang, X. Deng, and Q. Fan, *PLoS One*, **9**, 96 (2014).
57. J. Wang, *Analytical Electrochemistry, Third Edition*, 2006.
58. D. V. Navolotskaya, H. S. Toh, C. Batchelor-McAuley, and R. G. Compton, *ChemistryOpen*, **4**, 595 (2015).
59. R. Zhiani, M. Ghanei-Motlag, and I. Razavipanah, *J. Mol. Liq.*, **219**, 554 (2016).
60. J. Y. Liu and R. H. Hurt, *Environ. Sci. Technol.*, **44**, 2169 (2010).
61. S. J. Cloake, H. S. Toh, P. T. Lee, C. Salter, C. Johnston, and R. G. Compton, *ChemistryOpen*, **4**, 22 (2015).
62. X. Li, C. Batchelor-McAuley, and R. G. Compton, *ACS Sensors*, **44**, acssens-8b01482 (2019).